

New sub- μ s isomers in $^{125,127,129}\text{Sn}$ and isomer systematics of $^{124-130}\text{Sn}$

R. L. Lozeva,^{1,2,3,*} G. S. Simpson,^{4,5} H. Grawe,⁶ G. Neyens,¹ L. A. Atanasova,² D. L. Balabanski,^{7,8,9} D. Bazzacco,¹⁰ F. Becker,⁶ P. Bednarczyk,^{6,11} G. Benzoni,¹² N. Blasi,¹² A. Blazhev,¹³ A. Bracco,^{12,14} C. Brandau,¹⁵ L. Cáceres,^{6,16} F. Camera,^{12,14} S. K. Chamoli,¹⁷ F. C. L. Crespi,^{12,14} J.-M. Daugas,¹⁸ P. Detistov,² M. De Rydt,¹ P. Doornenbal,^{6,13} C. Fahlander,¹⁹ E. Farnea,¹⁰ G. Georgiev,³ J. Gerl,⁶ K. A. Gladnishki,^{2,8} M. Górska,⁶ J. Grębosz,^{6,11} M. Hass,¹⁷ R. Hoischen,¹⁹ G. Ilie,^{13,20} M. Ionescu-Bujor,²⁰ A. Iordachescu,²⁰ J. Jolie,¹³ A. Jungclaus,¹⁶ M. Kmiecik,¹¹ I. Kojouharov,⁶ N. Kurz,⁶ S. P. Lakshmi,¹⁷ G. Lo Bianco,^{7,8} S. Mallion,¹ A. Maj,¹¹ D. Montanari,^{12,14} O. Perru,¹⁸ M. Pfützner,²¹ S. Pietri,¹⁵ J. A. Pinston,⁴ Zs. Podolyák,¹⁵ W. Prokopowicz,⁶ D. Rudolph,¹⁹ G. Rusev,²² T. R. Saitoh,⁶ A. Saltarelli,^{7,8} H. Schaffner,⁶ R. Schwengner,²² S. Tashenov,⁶ K. Turzó,¹ J. J. Valiente-Dobón,²³ N. Vermeulen,¹ J. Walker,^{6,15,16} E. Werner-Malento,⁶ O. Wieland,¹² and H.-J. Wollersheim⁶

¹*Instituut voor Kern- en Stralingsfysica, Katholieke Universiteit Leuven, B-3001 Leuven, Belgium*

²*Faculty of Physics, University of Sofia "St. Kl. Ohridski," BG-1164 Sofia, Bulgaria*

³*CNRSM, Université Paris-Sud, CNRS/IN2P3, F-91400 Orsay-Campus, France*

⁴*LPSC, Université Joseph Fourier Grenoble 1, CNRS/IN2P3, Institut National Polytechnique de Grenoble, F-38026 Grenoble Cedex, France*

⁵*Institut Laue-Langevin, F-38042 Grenoble Cedex 9, France*

⁶*Gesellschaft für Schwerionenforschung, D-64291 Darmstadt, Germany*

⁷*Dipartimento di Fisica, Università degli Studi di Camerino, I-62032 Camerino, Italy*

⁸*INFN Sezione di Perugia, I-06123 Perugia, Italy*

⁹*Institute for Nuclear Research and Nuclear Energy, Bulgarian Academy of Sciences, BG-1784 Sofia, Bulgaria*

¹⁰*Università degli Studi di Padova and INFN, Sezione di Padova, I-35122 Padova, Italy*

¹¹*Henryk Niewodniczański Institute of Nuclear Physics, Polish Academy of Sciences, PL-31342 Krakow, Poland*

¹²*INFN Sezione di Milano, I-20133 Milano, Italy*

¹³*Institut für Kernphysik, Universität zu Köln, D-50937 Köln, Germany*

¹⁴*Università degli Studi di Milano, I-20133 Milano, Italy*

¹⁵*University of Surrey, Guildford, Surrey GU2 7XH, United Kingdom*

¹⁶*Departamento de Física Teórica, Universidad Autónoma de Madrid, E-28049 Madrid, Spain*

¹⁷*Weizman Institute of Science, 76100 Rehovot, Israel*

¹⁸*CEA/DIF/DPTA/SPN, Bruyères le Châtel, F-91297 Arpajon Cedex, France*

¹⁹*Department of Physics, Lund University, S-22100 Lund, Sweden*

²⁰*National Institute for Physics and Nuclear Engineering, RO-76900 Bucharest, Romania*

²¹*Institute of Experimental Physics, Warsaw University, PL-00681 Warsaw, Poland*

²²*Institut für Strahlenphysik, Forschungszentrum Dresden-Rossendorf, D-01314 Dresden, Germany*

²³*INFN Laboratori Nazionali di Legnaro, I-35020 Legnaro, Italy*

(Received 27 March 2008; published 17 June 2008)

New sub- μ s isomers have been observed in the neutron-rich Sn isotopes. $^{125,127,129}\text{Sn}$ nuclei have been produced in a relativistic fission reaction of ^{238}U on a ^9Be target at 750 A·MeV and by the fragmentation of ^{136}Xe at 600 A·MeV populating high-spin yrast states. In addition to the already known μ s isomers, three new ones with sub- μ s half-lives have been observed. These yrast isomers are the high-spin members of the $\nu(d_{3/2}^{-1}h_{11/2}^{-2})$ and $\nu h_{11/2}^{-n}$, seniority $\nu = 3$ multiplets leading to isomeric ($23/2^+$) and ($27/2^-$) states, respectively. Added to the already known $19/2^+$ μ s isomers in this region the current work completes the systematic information of neutron-hole excitations toward the filling of the last $h_{11/2}$ orbital at $N = 82$. The results are discussed in the framework of state-of-the-art shell-model calculations using realistic interactions.

DOI: [10.1103/PhysRevC.77.064313](https://doi.org/10.1103/PhysRevC.77.064313)

PACS number(s): 21.10.Tg, 21.60.Cs, 23.20.Lv, 27.60.+j

I. INTRODUCTION

Nuclei close to double shell closures offer an ideal environment for testing realistic shell-model calculations as these nuclei have a particularly simple structure: just a few particles or holes outside an inert core. Isomeric states are abundant in Sn isotopes with a few neutron holes away from ^{132}Sn . They are typically formed by yrast spin traps and allow the

observation of decay cascades in exotic nuclei. Such isomeric states exist because of the short-range, repulsive character of the nucleon-nucleon interaction for alike nucleons, which leads to small level spacings between the highest-spin states of a multiplet where the wave functions of the nucleons are not allowed to reach maximum overlap due to the Pauli principle. The unique-parity $h_{11/2}$ neutron-hole orbital, which lies close to the Fermi surface, is responsible for exactly this type of isomerism in nuclei near ^{132}Sn with $N < 82$.

To date, intermediate-spin states have been observed, in the Sn isotopes at, or a few neutrons away from, stability by using

*Radomira.Lozeva@csnsm.in2p3.fr

deep-inelastic reactions [1–4]. Further away from stability, Sn nuclei and their vicinity have been studied by using relativistic fission [5–7] and fragmentation [8,9] reactions. Intermediate-spin states were observed either directly after in-flight mass separation of μs isomeric states, produced by thermal neutron-induced fission [10–12], or by the β decay of intermediate-spin long-lived (seconds) In isomers [13,14]. The aforementioned experiments have allowed the complete $\nu h_{11/2}^{-n}$, seniority $\nu = 2$ multiplet to be measured for even-mass Sn isotopes in the mass range $A = 116$ –130. In these nuclei the filling of the $h_{11/2}$ orbital is not isolated. The presence of, for example, the close lying $d_{3/2}$ orbital leads to a delayed filling of the $h_{11/2}$ orbital as nucleons can scatter into it. The filling of the lower half of the $h_{11/2}$ orbital could well be enhanced due to scattering from the lower lying $g_{7/2}$, $d_{5/2}$, $s_{1/2}$ orbitals, which in total leads to deviations from the symmetric $B(E2)$ trend in an isolated high-spin orbital [15,16].

In addition to the $\nu = 2$ states, $\nu h_{11/2}^{-n}$, $\nu = 3$ isomeric states were also observed by using deep-inelastic reactions for $^{119,121,123}\text{Sn}$ [2]. These isomers, however, were not observed in the more neutron-rich Sn isotopes using fission reactions, as β decay cannot populate such high-spin states and their predicted lifetime of ~ 200 ns is below the observational limit of the Lohengrin mass spectrometer at the ILL, where the flight time is around $2 \mu\text{s}$ [10]. Valuable information about intermediate-spin states in the heavy odd Sn nuclei was however obtained from the decay of $\nu h_{11/2}^{-2} d_{3/2}^{-1}$ μs isomeric states [10–12]. In order to complete the systematic data for the $\nu h_{11/2}^{-n}$, $\nu = 3$ isomers, to see whether their $B(E2)$ values fit into the trend of the $\nu = 2$ isomers, and to gain more information on intermediate-spin states in these nuclei, data from a recent experimental campaign using relativistic fission or fragmentation performed at the fragment separator (FRS) at GSI [17] were examined, where the flight time of the reaction products was around 300 ns.

The new isomeric states were interpreted by using shell-model calculations performed with a realistic interaction derived from the CD-Bonn nucleon-nucleon potential [18]. A good description of the experimental data is found from using an effective neutron charge of $e_n = 0.70e$, in agreement with previous work in this region [19,20], and at variance with the larger values found in Refs. [3,12,21]. The experimental method and results are introduced in Secs. II and III, respectively, followed by an interpretation of these results in terms of probable configurations of the states involved in the decay sequence in Sec. IV.

II. EXPERIMENTAL DETAILS

Delayed γ rays from neutron-rich Sn isotopes were observed at the final focal point of the FRS [17] by using eight Cluster detectors [22] from the RISING array [23]. The experimental setup, shown schematically in Fig. 1(a), was used for the study of g factors of μs isomeric states as part of the g -RISING campaign [24].

The Sn nuclei were produced in two separate experimental runs: by relativistic projectile fission of a 750 A·MeV ^{238}U beam, with an intensity of $\sim 8 \times 10^7$ ions/s impinging on

a 1023 mg/cm² Be primary target (with Nb backing of 221 mg/cm²), and by the fragmentation of a ^{136}Xe beam, with an intensity of $\sim 2 \times 10^8$ ions/s impinging on the same target at 600 A·MeV [25].

The reaction products were identified by the FRS, which was set up in a standard achromatic configuration [17]. Mass identification of the ions was performed by an event-by-event measurement of the magnetic rigidity ($B\rho$) at the dispersive (middle) focal plane and the velocity, determined in a time-of-flight (ToF) measurement by using position-sensitive scintillators placed at middle (Sc1) and final (Sc2) focuses of the spectrometer. Z determination was performed by measurements of the energy loss in an ionization chamber (MUSIC), while (x, y) tracking of the ions was achieved by using two multiwire proportional counters (MW1 and MW2).

Ions entering the gap of the magnet used for g -factor studies were also detected by a scintillation detector (validation), whose signal was required for the acceptance of an ion- γ coincidence event in the analysis. The ions, after being slowed through 15 mm of Plexiglass, were stopped in a 2 mm thick Cu catcher placed at the center of the magnet's poles. A scintillator (veto) placed behind the catcher was used to reject ions passing through it. To adjust the implantation depth in the Cu foil a variable-thickness Al degrader was used at the final focus.

The Ge detector setup, where all Cluster detectors were placed in the horizontal plane shown in Fig. 1(a), had a γ -ray detection efficiency of 2.2% at 500 keV and 1.8% at 1.3 MeV. Add-back of up to three (out of seven) neighboring crystals in each Cluster was performed, chosen after a study of the best peak/background ratio. A time restriction for prompt γ rays for single crystals with Cluster multiplicity one was used in the analysis. Wider time and multiplicity restrictions were performed for the add-back energies. Half of the detectors were used with their BGO anti-Compton suppression shields [26] in place. To suppress the low-energy atomic bremsstrahlung associated with the arrival of the beam [23], all detector faces were covered by Cu and Pb absorbers, each 1 mm thick. This provided a useful γ -ray energy detection range of between ~ 140 keV and ~ 4 MeV, the upper limit being due to the selected ADC range of the used Euroball VXI cards. Ion- γ coincidences were accepted up to 15.4 μs after the arrival of an ion and were measured by using a common TAC, started by the first γ ray measured in any of the Ge detectors, and stopped by a delayed signal from scintillator Sc2. Times between the first γ ray, detected within the ion- γ time window, and any other coincident γ rays were measured by a TDC, which had a range of 1.2 μs . The constant fraction discriminators (CFDs) of the Ge detectors were inhibited for the first 300 ns after the arrival of an ion to avoid the TDC time window being opened by the prompt atomic bremsstrahlung from the beam. The time resolution of the Ge detectors was ~ 20 ns.

Electronics effects such as the blocking effect of the Ge detectors' CFDs and the sharp end of the coincidence gate for particles and γ rays limit the useful range for time analysis to between 800 ns and 14.6 μs , respectively. During the suppression of the prompt background (BG) radiation in the first few hundreds of nanoseconds, when the Ge detectors' CFDs recover, a short-lived isomeric radiation can be observed more clearly and with a higher intensity. Therefore, this time range

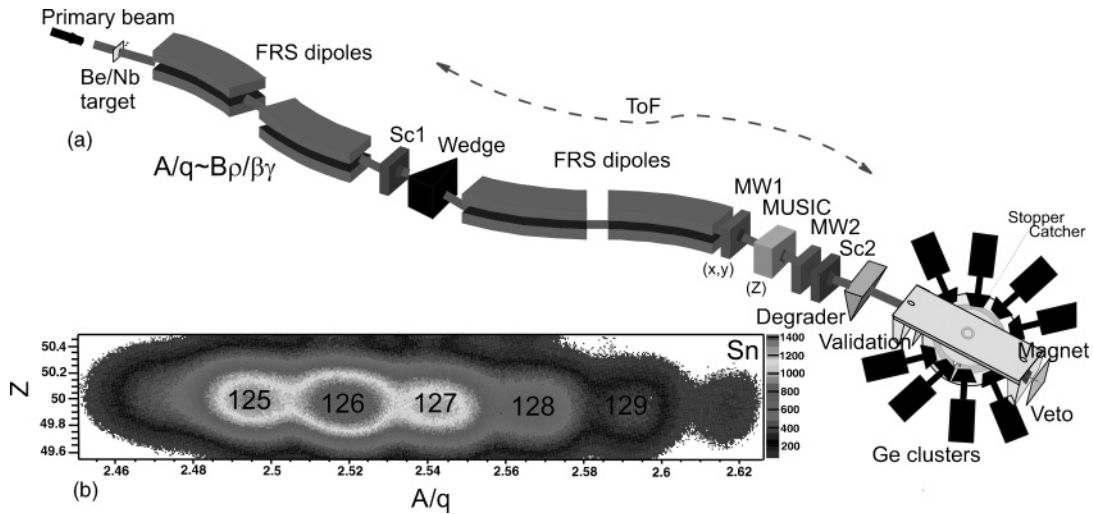


FIG. 1. (a) Experimental setup and (b) the identified Sn isotopes from ^{238}U fission.

is used only for visualization, whereas all time analysis starts 800 ns after the arrival of the ions, as will be shown in Sec. III.

III. ANALYSIS AND RESULTS

A. Notes about the background

Because of the high bombarding energies, the large amount of material close to the detectors (electromagnet), and the high ion rates (typically $\sim 5 \times 10^3$ ions/s) the nuclear BG

detected in the Ge detectors is rather high. Over short time ranges the main contribution to the BG comes from (n, γ) reactions in the Ge or/and the surrounding materials (Fe and Al) including the catcher itself (Cu). Most of these contributions are prompt, however, a certain amount persists at longer times. Additionally, the photopeaks at low γ -ray energy “sit” on a continuous BG from Compton scattering of higher energy γ rays. Therefore, an accurate background subtraction is important for the analysis. The single γ -ray spectra of

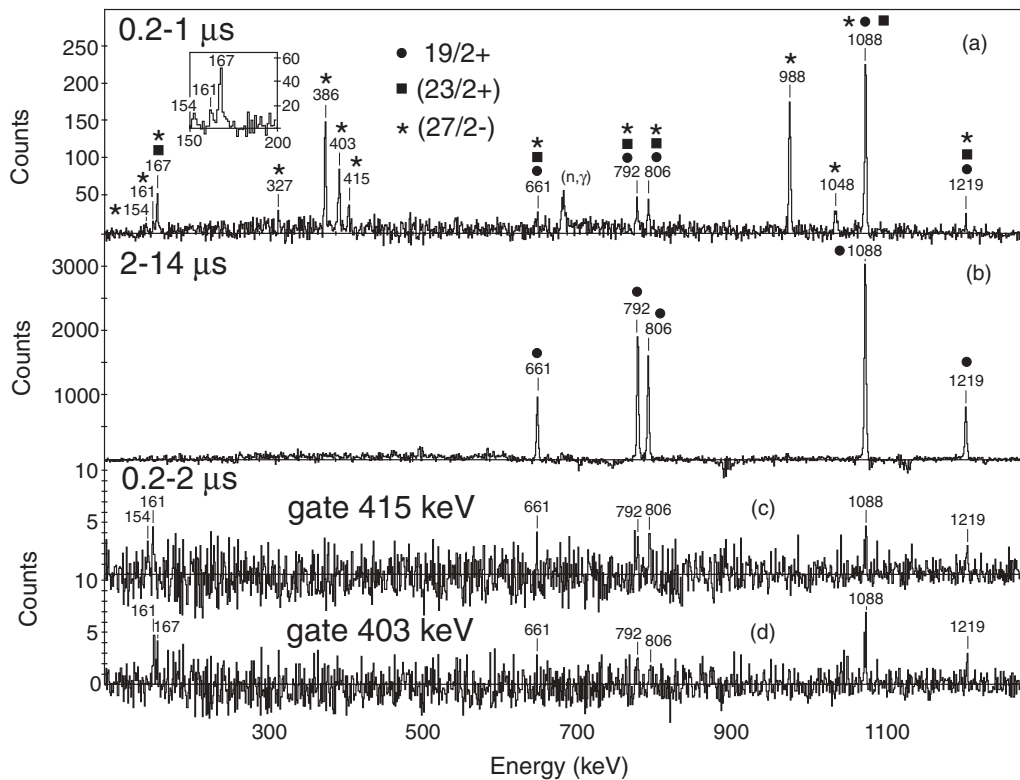


FIG. 2. BG-subtracted γ -ray spectra for time windows of (a) 0.2–1 μ s and (b) 2–14 μ s and coincident with (c) 415 keV and (d) 403 keV γ rays correlated with ^{125}Sn from ^{238}U fission.

odd- A nuclei [see, e.g., Figs. 2(a) and 2(b)] are cleaned of these BG contributions (present in the energy spectra of all nuclei) by subtracting a normalized portion from their even- A neighbors, whereas for the coincidence γ -ray spectra [see, e.g., Figs. 2(c) and 2(d)] a subtraction of the BG for the total energy projection is performed by using the methods described in Refs. [27,28]. The time structure of the BG is investigated over the entire energy range. Such an analysis reveals a mean half-life of 0.33(4) μ s, dominated mostly by the short-lived neutron-knockout activities. Therefore, a proper BG subtraction is essential. The experimental procedure was verified for several long-lived BG activities, for example, for the 198.4 keV line in ^{71}Ge ($T_{1/2} = 20.4$ ms [29,30]) and the 1460.9 keV line in ^{40}K ($T_{1/2} = 1.25 \times 10^9$ yr [31]) and, as expected, a constant time spectrum is observed.

The data analysis was performed by using SPY/CRACOW [32], ROOT [33], and the RADWARE [34] packages.

B. Odd-mass Sn nuclei

The isotopic identification of the Sn nuclei transmitted by the FRS is depicted in Fig. 1(b), where the atomic number Z is represented as a function of the mass/charge ratio (A/q). The spectrometer was tuned to optimally select ^{126}Sn , leading to a similar but reduced production and transmission of $^{125,127}\text{Sn}$ as well. The ToF measurement with Sc1 [Fig. 1(a)] was influenced by the high ion rates at the middle focus of the separator, which led to slightly overlapping distributions for the neighboring isotopes. Therefore, the corresponding contaminations of the odd Sn isotopes were removed in the analysis by subtracting a normalized portion from their even neighbors.

The relativistic fission and fragmentation reactions can populate high-spin states. Their decay proceeds toward states near the yrast line, some of which can be μ s isomers in the Sn region. In the following sections we confirm the μ s lifetimes of known isomers in $^{125,127,129}\text{Sn}$ and report on a new sub- μ s isomer in each of these isotopes.

1. ^{125}Sn

A new ($23/2^+$) isomer has been observed in ^{125}Sn , along with the previously known 0.23(3) μ s ($27/2^-$) and 6.2(7) μ s $19/2^+$ isomeric states reported in Refs. [1] and [10], respectively. The decay schemes of these isomers are confirmed in this work and four new transitions are added to the decay cascade out of the ($27/2^-$) isomer. The γ -ray spectrum in Fig. 2(a) shows the observed transitions in ^{125}Sn in a time window from 200 ns to 1 μ s after the arrival of the ion from the fission data set. It represents a BG-subtracted energy spectrum, taken shortly after the implantation, for which the contribution deduced from an equal time region at the end of the time range is canceled. The BG contributions are subtracted as explained in Sec. III A. As a result, the only remaining peak, not belonging to ^{125}Sn , that could not be fully removed by the BG subtraction comes from the strong short-lived 691.4 keV $^{72}\text{Ge}(n, \gamma)$ transition [35].

A BG-subtracted spectrum in a time range from 2 to 14 μ s from the same data set is presented in Fig. 2(b). All γ rays in the spectrum belong to the known decay of the $19/2^+$ isomer in ^{125}Sn [10].

Half-lives of 0.23(2) and 6.2(2) μ s are determined for the ($27/2^-$) and $19/2^+$ states, respectively, by using only the strongest transitions in the cascades for the lifetime determinations.

The ($23/2^+$) state has already been observed as an isomer in the neighboring $^{123,127,129}\text{Sn}$ nuclei [2,12,36]. Two previous experiments [1,10] studying ^{125}Sn at intermediate spin were unable to observe the ($23/2^+$) isomer due to poor particle identification and a lack of statistics, respectively.

The four newly observed γ rays of energies 154, 167, 403, and 415 keV are seen in Fig. 2(a). One has to note that these transitions have not been reported in the previous work for the ($27/2^-$) isomer in this nucleus [1], where only the direct depopulation of the ($27/2^-$) state, through the negative-parity states, could be observed.

The γ - γ coincidence relations from the current work are shown in Figs. 2(c) and 2(d). They are performed for the first 2 μ s of the time window after a BG subtraction (see Sec. III A). The coincidences with known transitions represent the corresponding feeding of the short-lived isomer and the consecutive decay of the longer lived one. By setting gates in a γ -time matrix, to extract time information about the new transitions, and also by observing the γ - γ coincidences it was possible to associate the 154, 403, and 415 keV transitions with the decay cascade out of the 0.23(2) μ s ($27/2^-$) isomer alone and the 167 keV transition with the decay out of another lower lying isomer. The 154 keV γ ray is in coincidence with the 415 keV transition [Fig. 2(c)]. If the sum of these two γ -ray energies is added to the energy of the 1894 keV $19/2^+$ isomer an energy of 2463 keV is obtained, the same as that of the ($23/2^-$) state reported in Ref. [1]. The 154 keV transition is associated with the decay out of the ($23/2^-$) level and the 415 keV with the decay of a ($21/2^+$) state [see Sec. IV B1].

The newly observed 167 keV transition has a half-life of 0.6(2) μ s [Fig. 3(b)], which is inconsistent with any of the known isomers in this nucleus. This transition is also in coincidence with the 403 keV γ ray [Fig. 2(d)]. The sum of these two transitions and the 1894 keV $19/2^+$ isomer also gives 2464 keV, which is the energy of ($23/2^-$) state from Ref. [1]. The 403 keV transition is therefore postulated to be another decay out of the ($23/2^-$) level.

The ground state (g.s.) 1088 keV transition in the fission data was fitted with three decay components [in the inset of Fig. 3(b)], consistent with the three observed isomeric decays in ^{125}Sn . It is interesting to note that the strong direct decay of the ($27/2^-$) isomer is visible from the pronounced hump at the beginning of the spectrum. This decay branch is considerably reduced in the heavier Sn isotopes as, for example, visible from the decay curve for the 1095 keV transition in ^{127}Sn [in the inset of Fig. 3(d)] and the 1136 + 570 keV transitions in ^{129}Sn [Fig. 3(f)]. A detailed comparison of the isomeric population from both fission and fragmentation data sets will be the subject of a forthcoming article.

2. ^{127}Sn

Isomeric $19/2^+$ and $23/2^+$ states with half-lives of 4.5(3) and 1.26(15) μ s, respectively, were previously reported in

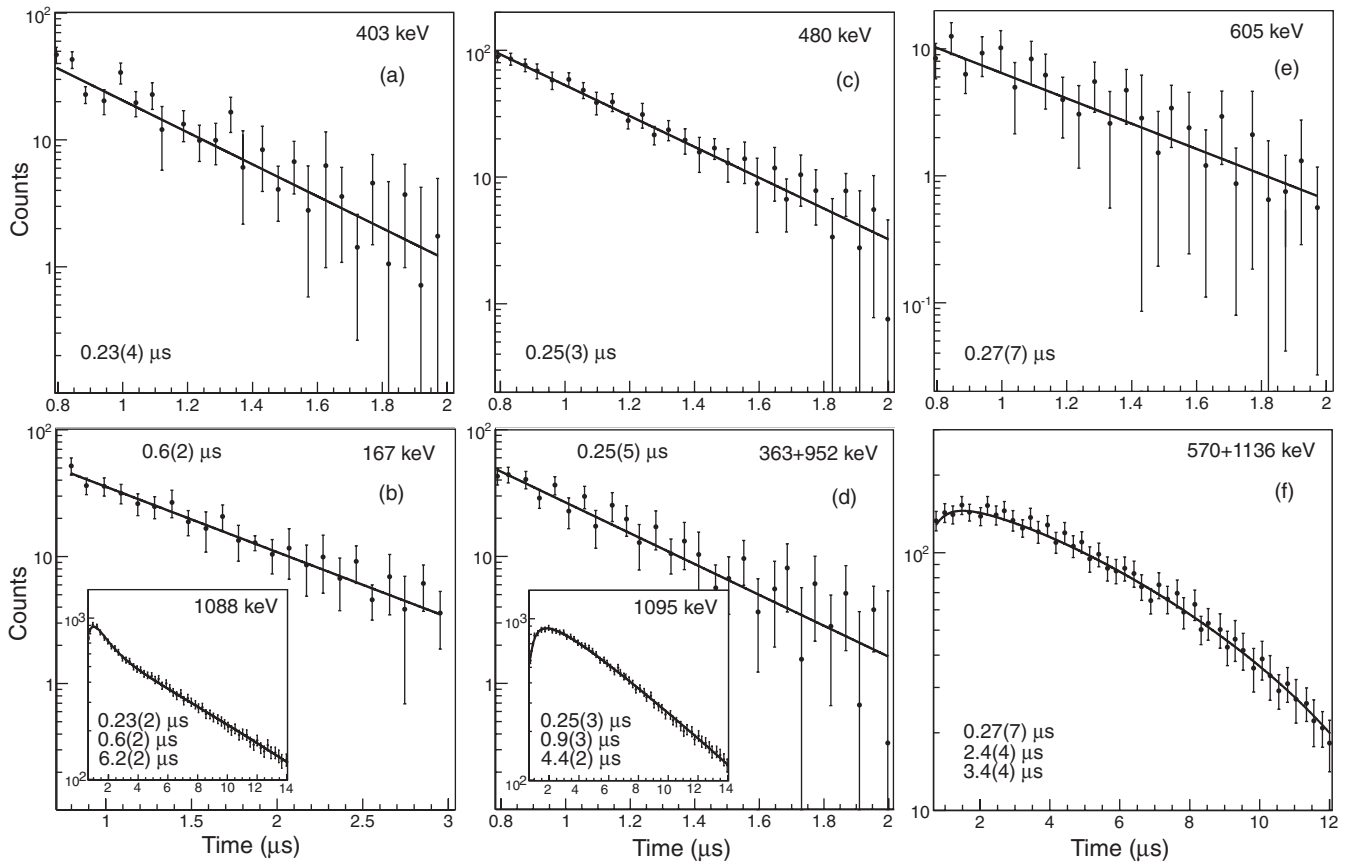


FIG. 3. Decay curves for the newly observed γ transitions in (a and b) ^{125}Sn , (c and d) ^{127}Sn , and (e) ^{129}Sn from ^{238}U fission. The decay curves of the g.s. transitions in the three nuclei are shown in the insets of (b) and (d) and in (f).

Refs. [10,36]. The decay scheme of the $19/2^+$ isomer is confirmed in this work, although the $23/2^+$ isomer decaying by a 104 keV isomeric transition was not observed due to the low efficiency of the Ge detector setup at such low γ -ray energies. In addition to these two isomers in ^{127}Sn , a new $(27/2^-)$ isomer with a half-life of $0.25(3) \mu\text{s}$ and four associated delayed γ rays at energies of 142, 363, 480, and 952 keV are seen in this work. All new transitions are present in the BG-subtracted energy spectrum, taken shortly after the implantation (similar to ^{125}Sn in Fig. 4(a)), which represents data from both ^{238}U fission and ^{136}Xe fragmentation. This isomer was not observed in previous isomer studies of this nucleus [10], due to its short half-life, and was not populated in β -decay studies [36], due to its high spin.

The four newly observed transitions can be assigned to the decay cascade of a new $(27/2^-)$ isomer by measurements of their half-lives [Figs. 3(c) and 3(d)] and observations of γ - γ coincidences [Figs. 4(c)–4(e)], which also permitted the level scheme construction. The new 2410 keV level is obtained by summing the 363, 952, and known 1095 keV transitions, which are observed in mutual coincidence. The 363 and 952 keV γ rays have similar intensities (see Table I). The sum of the 1931 keV $23/2^+$ isomeric level and the new 480 keV transition also gives a similarly consistent energy of 2411 keV. Note that a 952 keV transition was observed in β -decay studies [36] and placed in the decay scheme

in a cascade with the 1095 keV transition. However, no spin-parity (I^π) suggestions for this state were made. The newly observed 142 keV transition is in coincidence with all other new transitions [Fig. 4(c)] and is very likely the isomeric $(27/2^-) \rightarrow (23/2^-)$ transition. The extended level scheme for ^{127}Sn is shown in Fig. 3(b) and is discussed in Sec. IV B2.

3. ^{129}Sn

Two new γ rays of 145 and 605 keV have been observed in the BG-subtracted energy spectrum for ^{129}Sn , taken shortly after the implantation [Fig. 5(a)], in the same way as those for ^{125}Sn and ^{127}Sn . The data from both ^{238}U fission and ^{136}Xe fragmentation experiments were added to obtain better statistics. As in ^{125}Sn , the only remaining peak, not belonging to ^{129}Sn , comes from the strong short-lived 691.4 keV line $^{72}\text{Ge}(n, \gamma)$ [35], which could not be perfectly subtracted.

The two newly observed transitions are assigned to the decay of a new $0.27(7) \mu\text{s}$ ($27/2^-$) isomer [Fig. 3(e)]. Because of the thick absorbers and the low efficiency of the setup at energies around 140 keV the half-life of this isomer could be extracted only from the 605 keV transition after an appropriate BG subtraction. The obtained result was in addition verified by using a double exponential fit for the non-BG subtracted data to account for the exponential BG present at short times

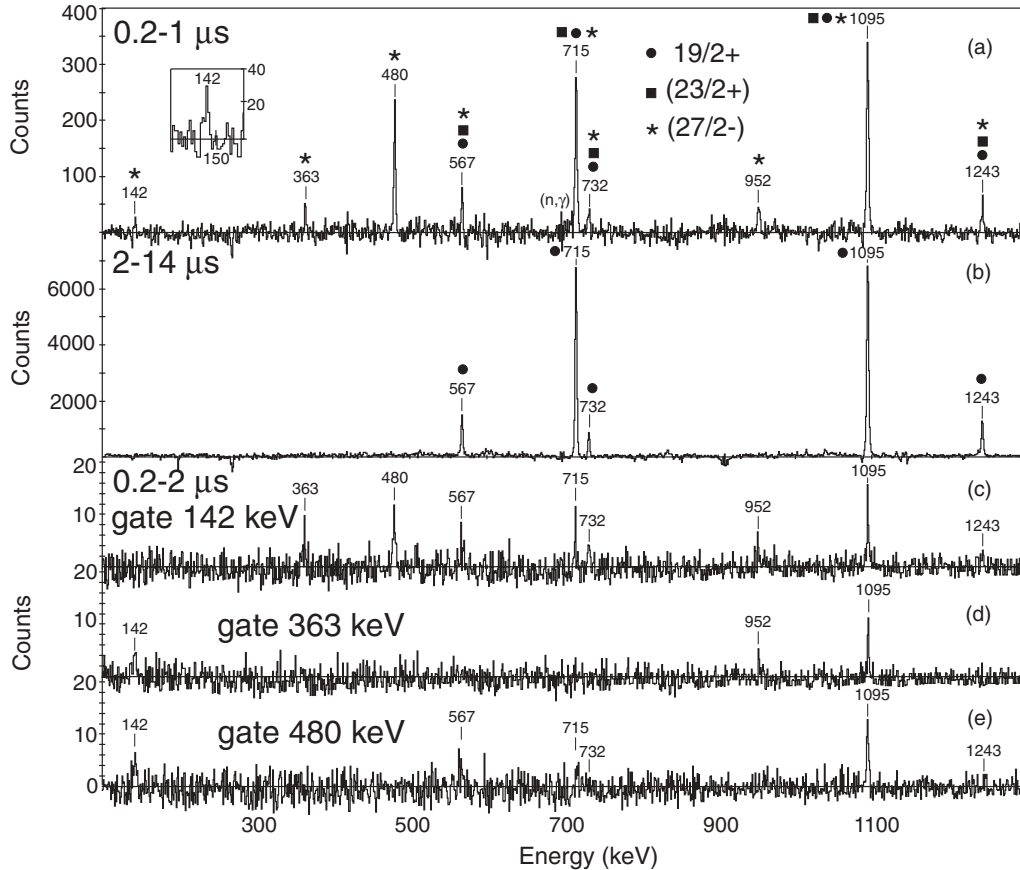


FIG. 4. BG-subtracted γ -ray spectra for time windows of (a) 0.2–1 μ s and (b) 2–14 μ s and coincident with (c) 142 keV, (d) 363 keV, and (e) 480 keV γ rays correlated with ^{127}Sn from ^{238}U fission and ^{136}Xe fragmentation.

from neutron activities (see Sec. III A). The given uncertainty for the half-life value includes the statistical one from such an analysis.

The previously reported level schemes of Refs. [12,36] are confirmed here, though the low-energy decays of the 3.6(2) μ s $19/2^+$ isomer (19.7 keV) and the 2.4(2) μ s $23/2^+$ isomer (41.0 keV) were not observed. A BG-subtracted energy spectrum from the end of the time range (as for ^{125}Sn and ^{127}Sn) is presented in Fig. 5(b). All γ rays labeled with their energy belong to the known decay of the $19/2^+$ isomer in ^{129}Sn [12].

Due to the lack of statistics for this nucleus a summed coincidence spectrum was constructed with gates on all known (and the new 605 keV) transitions [Fig. 5(c)]. In this spectrum, the 145 keV transition is clearly visible, supporting its placement as $(27/2^-) \rightarrow (23/2^-)$ in analogy to the 142 and 161 keV transitions in ^{127}Sn and ^{125}Sn , respectively.

IV. DISCUSSION

The half-lives obtained in the current data set are compared with the existing data in Table I, where one can notice a good agreement. The measured energies of all observed γ -ray transitions and their absolute intensities, normalized to the

most intense one for each nucleus, are listed for each isomeric state.

Additionally, all μ s isomers in the even- A $^{124,126,128,130}\text{Sn}$ isotopes were remeasured. The half-lives obtained for the 10^+ , 7^- (in $^{124,126}\text{Sn}$), and 5^- (in ^{124}Sn) isomeric states are fully in agreement with the literature values [1,3,11,13,37]. Therefore, the lifetimes in the even Sn isotopes are used only for the odd-even renormalization of the reduced transition probabilities (see Sec. IV E).

A. Shell-model calculations

Shell-model (SM) calculations are performed in a model space $p_{1/2}$, $g_{9/2}$ for protons and $g_{7/2}$, $s_{1/2}$, $d_{5/2}$, $d_{3/2}$, $h_{11/2}$ for neutrons outside an inert ^{88}Sr core. Therefore, proton-core excitations across $Z = 50$ and neutron-core excitations across $N = 82$ are not considered in this approach. The polarization by proton-core excitations for a well-tuned realistic interaction has a negligible impact on the level energies, but its effect on the γ -ray transition rates, in general, comprises the use of effective operators. For specific transitions, however, namely weak ones, major discrepancies may occur owing to the restriction to a pure neutron configuration space. Starting from the G matrix, including folded diagrams and higher order

TABLE I. Isomeric half-lives and γ -ray transitions observed in the decay of the ^{125}Sn , ^{127}Sn , and ^{129}Sn isomers ($\Delta E_\gamma \sim 0.3$ keV, $\Delta I_\gamma \sim 10\%$). The intensities of all low-energy transitions could not be obtained due to the high uncertainty in the extrapolation of the efficiency curve.

Nucleus	State	Literature	$T_{1/2}(\mu\text{s})$		E_γ (keV) (I_γ)
			This work	Adopted	
^{125}Sn	$27/2^-$	0.23(3) ^a	0.23(2)	0.23(2)	154.0, 161.3, 326.7 (9), 385.9 (46), 402.9 (30), 415.3 (15), 988.4 (45), 1048.3 (9)
^{125}Sn	$23/2^+$	—	0.6(2) ^c	0.6(2)	167.0
^{125}Sn	$19/2^+$	6.2(7) ^b	6.2(2)	6.2(2)	661.5 (29), 791.6 (55), 805.5 (45), 1087.7 (100), 1219.0 (25)
^{127}Sn	$27/2^-$	—	0.25(3) ^c	0.25(3)	142.0, 363.1 (16), 952.3 (16), 479.7 (57)
^{127}Sn	$23/2^+$	1.26(15) ^c	0.9(3)	1.2(1)	—
^{127}Sn	$19/2^+$	4.5(3) ^b , 4.8(3) ^c	4.4(2)	4.5(1)	567.1 (20), 715.4 (85), 731.8 (15), 1094.9 (100), 1242.6 (19)
^{129}Sn	$27/2^-$	—	0.27(7) ^e	0.27(7)	145.3, 605.0 (97)
^{129}Sn	$23/2^+$	2.0(2) ^c , 2.4(2) ^d	2.4(4)	2.2(1)	—
^{129}Sn	$19/2^+$	3.7(2) ^b , 3.2(2) ^c , 3.6(2) ^d	3.4(4)	3.4(1)	382.1 (69), 570.3 (100), 1136.1 (88), 1324.4 (65)

^aTaken from Ref. [1].

^bTaken from Ref. [10].

^cTaken from Ref. [36].

^dTaken from Ref. [12].

^eNewly observed isomer.

many-body corrections for this valence space, we can derive an effective interaction from the CD-BONN nucleon-nucleon (NN) potential with the method described in Ref. [38]. The evolution of the experimental single-particle energies in ^{88}Sr for proton holes and in ^{100}Sn for neutrons, as adopted from Refs. [15,39], is reproduced by applying monopole corrections. The effective interaction is found to describe very well both high-spin states and Gamow-Teller decays in the

^{100}Sn region [40]. For the ^{132}Sn region, besides $A^{-1/3}$ scaling, additional monopole corrections are applied to describe the single-hole energies in ^{132}Sn [15,39], without modifying the ^{100}Sn results. Transition strengths for $E2$, $E3$, $M1$, and $M2$ transitions were calculated with an effective charge $e_n = 0.70e$ and a quenched g factor $g_n^s = 0.7g_n^s$. Calculations were performed with the code OXBASH [41]. In the following mainly levels and $E2$ strengths will be discussed. A full account of all

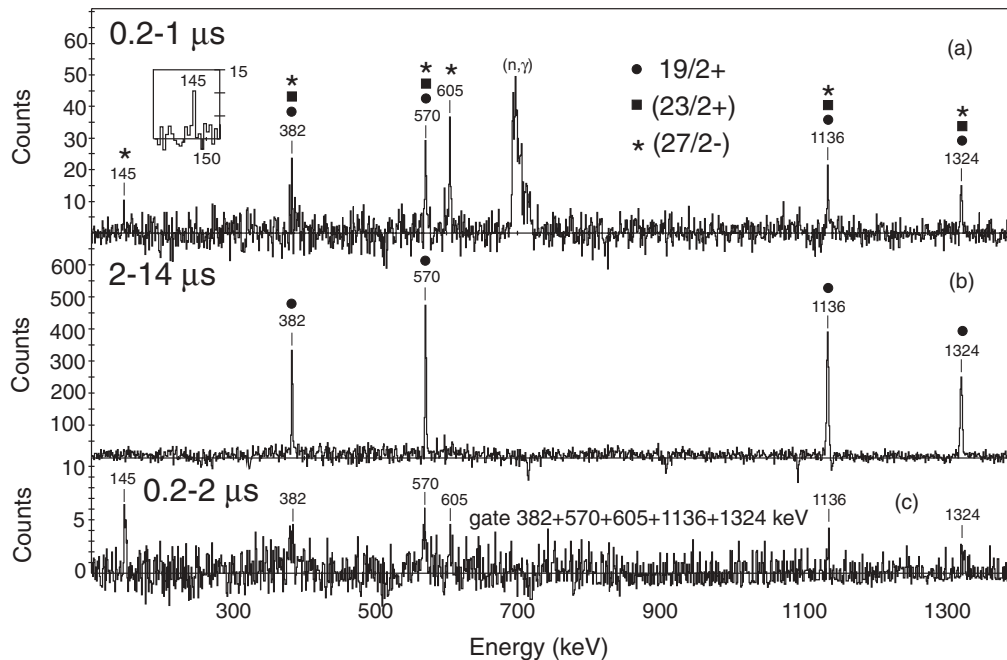


FIG. 5. BG-subtracted γ -ray spectra for time windows of (a) 0.2–1 μs and (b) 2–14 μs and coincident (summed-up) γ rays correlated with ^{129}Sn from ^{238}U fission and ^{136}Xe fragmentation.

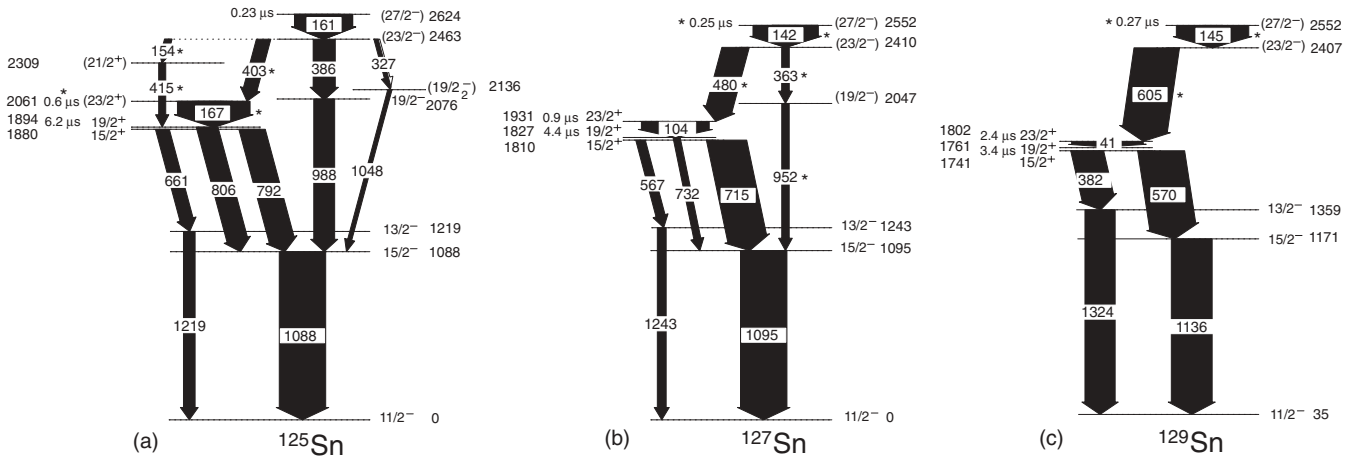


FIG. 6. Extended level schemes for (a) ^{125}Sn , (b) ^{127}Sn , and (c) ^{129}Sn . The newly observed γ lines and isomers are marked with asterisks. The intensities (represented by the arrow widths) for the low-energy transitions are estimated from balances with all other feeding/branching-transition intensities.

SM results in the ^{132}Sn region will be given in a forthcoming paper [42].

The results from the SM calculations are discussed in Sec. IV B. Level energies are compared with the experimental data in Figs. 7 and 8 and transition probabilities for selected $E2$ transitions are presented in Fig. 11 and Table II.

B. Level schemes

In Fig. 6 we present the extended level schemes, including the newly observed isomeric levels and their decay paths. Newly observed γ lines are indicated by asterisks. This is discussed further below for each case.

1. ^{125}Sn

The newly observed isomeric γ transitions of 154, 167, 403, and 415 keV in ^{125}Sn are placed in the extended level scheme, presented in Fig. 6(a), by using lifetime analysis and coincidence relations. Based on that, we suggest a new isomer of $I^\pi = (23/2^+)$, thus completing the $(23/2^+)$ systematics from ^{123}Sn [2] to $^{127,129}\text{Sn}$ [36]. The measured half-life is

in agreement with an $E2$ decay to the $19/2^+$ state from Weisskopf estimates (WE) and SM considerations and we place this level at 167 keV above the $19/2^+$ state. The other newly observed transitions correspond to the decay of the $(27/2^-)$ isomer toward the positive-parity states through two new intermediate states of $I^\pi = (21/2^+)$ and $I^\pi = (23/2^+)$. The $(19/2^-)$ states, suggested in Ref. [1], are consistent with our measurement.

The proposed level scheme is in full agreement with the SM calculations (Sec. IV A). The theoretical SM states for $^{125,127,129}\text{Sn}$ are compared with the experimental ones in Fig. 7 for both positive and negative parities. A good agreement is visible for the three nuclei of interest. In Figs. 7(a)–7(c) one can see that three of the states are candidates for yrast spin traps: $19/2^+$, $23/2^+$, and $27/2^-$. The highest spin yrast trap $27/2^-$ is populated directly in the reaction, whereas the other isomers are populated both directly and indirectly by feeding from the top isomer, which is consistent with our lifetime measurements. As can be seen, for example, in Fig. 7(a), where the decay path of the isomers in these nuclei is indicated with arrows, the decay from the $27/2^-$ trap is possible only by a low-energy $E2$ transition to the $23/2^-$ state with a half-life of about

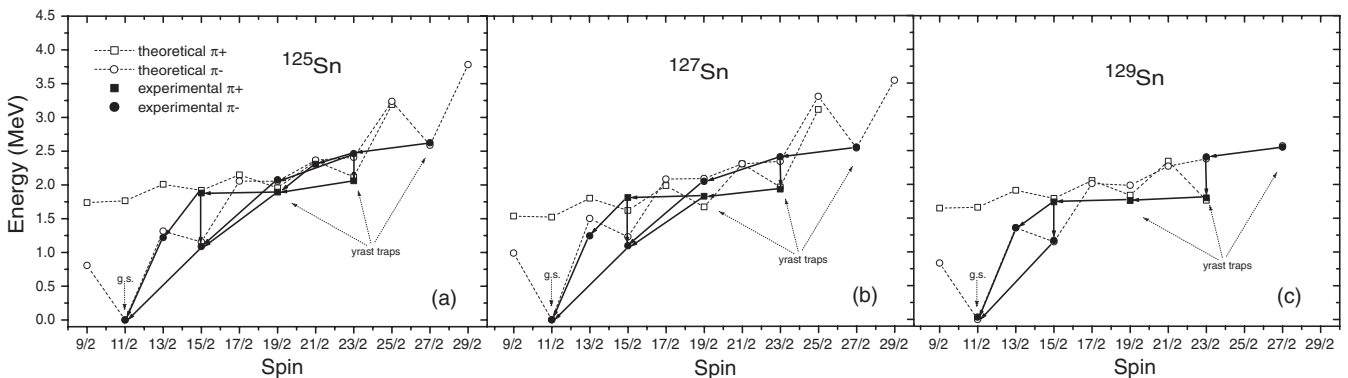


FIG. 7. Theoretical (empty symbols) and experimental (filled symbols) yrast states for (a) ^{125}Sn , (b) ^{127}Sn , and (c) ^{129}Sn for positive (squares) and negative (circles) parity. The decay path of the isomers in these nuclei is indicated with arrows.

200 ns, as indeed reported in Ref. [1] and observed in this work (see Table I). Due to the energy gap between the $23/2^-$ and the $23/2^+$ states, the isomeric decay proceeds most probably by an $E1$ branch toward the positive-parity states. The de-excitation of the $23/2^+$ state favors an $E2$ transition to the $19/2^+$ state, theoretically expected to be of 161 keV (from the SM energy level differences), which is experimentally found to be of 167 keV. The theoretically estimated half-life for this state is of the order of 500 ns, which agrees well with the experimental value of $0.6(2) \mu\text{s}$. The decay from the $19/2^+$ state proceeds through the $15/2^+$ state as well as the low-lying $13/2^-$ and $15/2^-$ states, as already known from the literature [10].

2. ^{127}Sn

All new isomeric transitions (142, 363, 480, and 952 keV) in ^{127}Sn , presented in Fig. 6(b), have the same half-life of $0.25(3) \mu\text{s}$, in agreement with the expected value of about 200 ns [10] for a new $(27/2^-)$ isomer in this nucleus. The 142 keV transition is coincident with all other transitions [Fig. 4(c)] and its energy is in agreement with an $E2$ decay to the $(23/2^-)$ state from WE and SM considerations. This transition was also suggested semiempirically to be of the order of 135(2) keV [10]. The cascade out of the new $(27/2^-)$ isomer is analogous to that in ^{125}Sn . The intensities of all isomeric decays however are distributed differently than those in the lighter Sn nuclei. The suggested experimental states in the proposed level scheme [Fig. 6(b)] match the theoretical SM states well, as can be seen in Fig. 7(b).

3. ^{129}Sn

The new isomeric γ transitions of 145 and 605 keV in ^{129}Sn are placed in the extended level scheme, presented in Fig. 6(c), by using lifetime analysis and coincidence relations. Thus, the new isomer of $I^\pi = (27/2^-)$ completes the systematics of known $(27/2^-)$ states from ^{119}Sn [2] to ^{129}Sn [36].

A comparison with the SM calculation (Sec. IV B) and empirical shell-model (ESM) estimates suggests that the 145 keV transition is very likely responsible for the isomerism whereas the 605 keV transition is assigned as the decay from the $(23/2^-)$ state to the $23/2^+$ state. In the ESM, if we assume pure $h_{11/2}^n$ configurations, the relative positions of the $23/2^-$ and $27/2^-$ states in ^{129}Sn can be calculated from the known 6^+ to 10^+ states in ^{130}Sn (see, e.g., Refs. [4,10,15]). The result for the $27/2^- \rightarrow 23/2^-$ transition energy is 135(2) keV (the same as for ^{127}Sn), where the systematic uncertainty is estimated from the configurational purity of the high-spin states involved in the full shell-model calculation. The 145 keV γ ray is the only candidate in that energy range seen in Fig. 5(a). This was confirmed in a follow-up experiment employing fragmentation of ^{136}Xe and a more efficient detector setup [43].

The 145 keV transition is placed at the top of the level scheme, suggesting that the new isomer of $I^\pi = (27/2^-)$ decays analogously to the ones in the lighter Sn nuclei, which is indeed expected from WE and SM predictions.

An $E2$ cascade out of the $(23/2^-)$ state can be suggested based on an ESM estimate in the spirit of Ref. [10], with the full

shell-model calculation and extrapolations from systematics to be of 307 and 929 keV (with a similar uncertainty as for the predicted 135 keV transition) for the $23/2^- \rightarrow 19/2^-$ and the $19/2^- \rightarrow 15/2^-$ transitions, respectively. Following the intensity distribution of the isomeric decays in the lighter odd- A neighbors, the observation of this cascade would require better statistics. Assuming the SM $E2$ decay energy and reduced transition strengths equal to ^{127}Sn would increase the $E1(605 \text{ keV})/E2(307 \text{ keV})$ branching by at least a factor of 5 relative to ^{127}Sn .

The suggested experimental states in the proposed level scheme [Fig. 6(c)] match the theoretical SM states quite well, as can be seen in Fig. 7(c). Thus, the decay of the $(27/2^-)$ isomer seems to be shifted toward the positive-parity states through the 605 keV transition. This is supported by the energy differences between the theoretically calculated states in Fig. 7(c), where the energy gap between the $23/2^- \rightarrow 23/2^+$ states is larger than the one between the $23/2^- \rightarrow 19/2^-$ states. The intensity of the 605 keV ($E1$) transition is also consistent with the increasing intensity of the branch toward the heavier masses, following the trend from $^{125,127}\text{Sn}$.

In conclusion, the following points summarize the decay of the three μs isomers in $^{125,127,129}\text{Sn}$:

- (i) The $(27/2^-)$ isomers decay through $E2$ cascades toward the negative-parity states in the lighter Sn nuclei. These branches become very weak as A increases.
- (ii) The decay path via $E1$ transitions from the $(23/2^-)$ to the $(23/2^+)$ levels toward the positive-parity states is enhanced, as the energy spacing between these states also increases with A .
- (iii) The energies of the $E2$ transitions from the $(27/2^-)$ to the $(23/2^-)$ levels stay almost constant, reflecting similar isomeric half-lives and pure configurations, whereas the excitation energy of the $27/2^-$ isomer is lowered toward $N = 82$.
- (iv) The $E2$ -transition energies of the $(23/2^+) \rightarrow 19/2^+$ de-excitation decrease with increasing A , whereas the $19/2^+ \rightarrow 15/2^+$ transition energy stays nearly constant.
- (v) The intensity distribution of the decays from the $19/2^+$ states differs significantly in the lower masses, where the feeding to the $15/2^-$ states is almost equally contributed to by transitions from the $19/2^+$ and $15/2^+$ states.
- (vi) In the heavier odd- A Sn nuclei, de-excitations from the $15/2^+$ states only are favored as the energy for a $19/2^+ \rightarrow 15/2^-$ transition decreases.
- (vii) Although in the lighter odd- A Sn isotopes the branches involving the $13/2^-$ states are weak, in the heavier A nuclei, these branches become dominant and even comparable with the branches involving the $15/2^-$ states.

C. High-spin states

1. $27/2^-$ states

A comparison between the energies of the calculated and the experimental $(27/2^-)$ and $(23/2^-)$ states is presented in

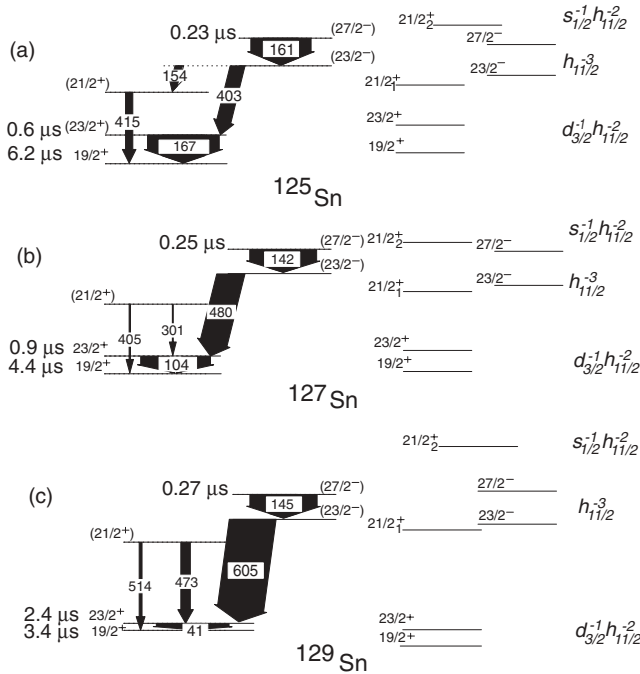


FIG. 8. Theoretical and experimental high-spin states. The transitions shown are from the current work and Ref. [36].

Fig. 8. According to the SM calculations, these states are the highest members of the $h_{11/2}^{-3}$ quasiparticle multiplet. For $A = 129$ the $h_{11/2}^{-3}$ probabilities in the wave functions are 100% and 99.5%, respectively. For the lighter isotopes the weights of the pure $h_{11/2}^{-n}$ configurations, with $n = 132 - A$, reduce to 32.4% and 28.4% for ^{127}Sn and 11.5% and 11.7% for ^{125}Sn due to pair scattering from the positive-parity g , d , s orbitals. As seniority is a good quantum number the total amount of $\nu = 3$ in the wave functions is more than 95%. The $23/2^-$, $19/2^-$, $15/2^-$, and $13/2^-$ excited states and the $11/2^-$ (g.s.) belong to the same multiplet. The $15/2^-$ and $13/2^-$ states have increasing admixtures of $d_{3/2}^{-1}s_{1/2}^{-1}h_{11/2}^{-1}$ and $d_{5/2}^{-1}s_{1/2}^{-1}h_{11/2}^{-1}$ quasiparticle configurations, respectively, which amount to about 30% and 15% in ^{129}Sn . This reflects the coupling of the $h_{11/2}$ particle to the 2^+ states in the neighboring even isotopes.

2. $23/2^+$ states

According to SM calculations, the yrast trap at spin $23/2^+$ (Fig. 7) has a dominant quasiparticle configuration of $\nu d_{3/2}^{-1}h_{11/2}^{-2}$, as discussed in Ref. [36]. In ^{125}Sn the dominant component is $\nu d_{3/2}^{-1}h_{11/2}^{-4}$ with 36.4%, while $\nu d_{3/2}^{-3}h_{11/2}^{-2}$ contributes with 22.0%. If only unpaired neutrons are considered, this is indeed the same type of quasiparticle configuration as in the heavier Sn, as discussed already in Ref. [36]. The leading quasiparticle configuration of $\nu d_{3/2}^{-1}h_{11/2}^{-2}$ in the heavier Sn, according to the calculations, has probabilities of 64.8% (^{127}Sn) and 97.0% (^{129}Sn). These numbers indicate the increasing purity of these states, as the seniority mixing

decreases, toward the filling of all involved orbitals at $N = 82$.

3. $21/2^+$ states

In ^{125}Sn we observe a state [Fig. 8(a)] and suggest $I^\pi = (21/2^+)$ based on the observation of this state in studies of the heavier Sn [36], which is also supported by theoretical calculations. The 2232 and 2275 keV levels [Figs. 8(b) and 8(c)] were assigned with a spin of $(21/2)$ in Ref. [36] for $A = 127$ and $A = 129$, respectively. The decay transitions to the $19/2^+$ and $23/2^+$ states, shown in Figs. 8(b) and 8(c), are taken from Ref. [36] and were not observed in the current data set due to insufficient statistics. The nonobservation of the branch from $23/2^-$ toward the $(21/2^+)$ state in ^{129}Sn is partly a consequence of the increasing energy of the $23/2^- \rightarrow 23/2^+$ transition, which is nicely reproduced by the SM calculations, while the distance between the $23/2^-$ and $21/2^+$ states stays essentially constant. This branch appeared in ^{125}Sn and transported about 15% of the total intensity from the $23/2^-$ state, compared to the 30% intensity of the $23/2^- \rightarrow 23/2^+$ branch. In the heavier mass nuclei the intensity is transported through the stronger $23/2^- \rightarrow 23/2^+$ transitions, which take about 76% (the 480 keV transition with respect to 363 keV transition) from the total intensity of the $23/2^-$ state in ^{127}Sn and 100% in ^{129}Sn (e.g., no branch other than the 605 keV transition is observed). In fact, the branches involving the $(21/2^+)$ states most probably become weaker as the mass increases and better statistics would be required to find out their exact contribution.

The $21/2_1^+$ states have a leading quasiparticle configuration of $\nu d_{3/2}^{-1}h_{11/2}^{-2}$ with a contribution of greater than 30% in ^{125}Sn [Fig. 8(a)] to above 96% in ^{129}Sn [Fig. 8(c)]. In the $21/2_2^+$ states the configuration involving the $\nu s_{1/2}$ orbital is enhanced and dominates (above 98%) in ^{129}Sn . For $A = 127$ [Fig. 8(b)], nevertheless, $\nu d_{3/2}^{-1}$ is dominant with 62.6% whereas in the lighter ^{125}Sn the $d_{3/2}$ and $s_{1/2}$ components are 20.5% and 35.1%, respectively. Note that the increased probability for hole excitation involving the $d_{3/2}$ orbital at $A = 127$ is reflected in the wave functions of all excited states [Fig. 8(b)].

D. Level systematics

The observation of three new isomers in the odd neutron-rich Sn isotopes allows a comparison with the information available on both the even and odd neutron-rich Sn nuclei. Such a plot representing the different origin of the isomeric states and the overall trend in the heavy Sn region is presented in Fig. 9(a).

Because of the closed proton shell at $Z = 50$ the decay schemes of the Sn nuclei originate mostly from neutron excitations across the subshells between the shell gaps at $N = 50$ and $N = 82$. The last $h_{11/2}$ orbital is strongly involved in single particle/hole excitations, represented by the seniority scheme [2,3]. The general features of the decays of the odd Sn ($^{125,127,129}\text{Sn}$) nuclei are quite similar to each other and to the lighter $^{119-121}\text{Sn}$, with the exception of ^{123}Sn ($N = 73$)-the half-filling point of the $h_{11/2}$ neutron orbital [3].

The μs isomeric states present in these nuclei originate from different configurations:

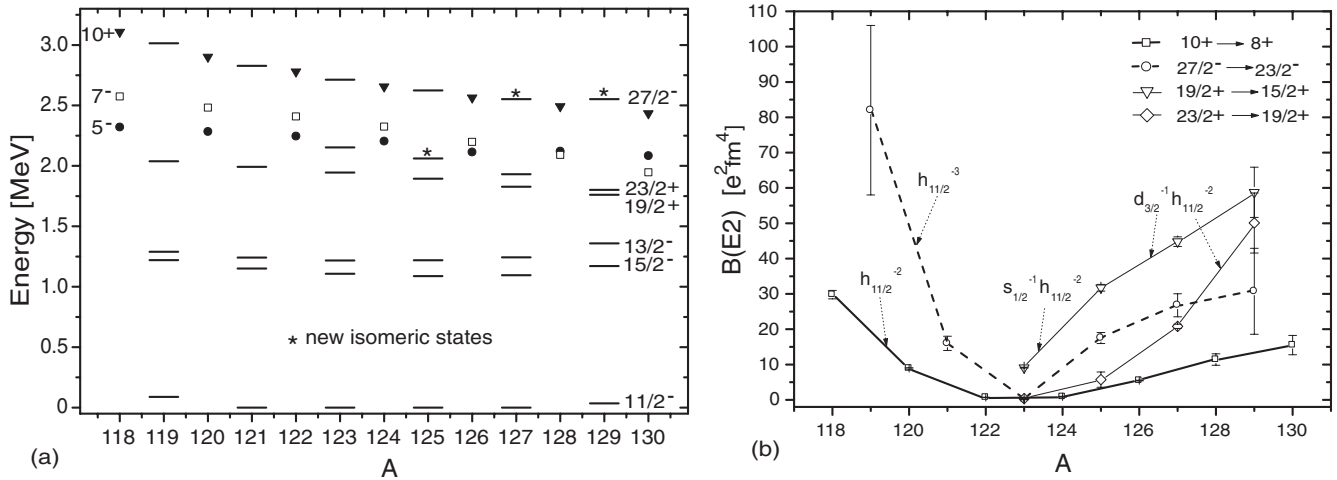


FIG. 9. (a) Systematics of the known and new (indicated by an asterisk) $19/2^+$, $23/2^+$, and $27/2^-$ isomeric states in the odd and even Sn isotopes. The first excited $15/2^-$ and $13/2^-$ states are given for comparison together with the $11/2^-$ g.s. (with exceptions for $^{119,129}\text{Sn}$, where $1/2^+$ and $3/2^+$ become the g.s., respectively). (b) Experimental $B(E2)$ values for the total $h_{11/2}$ shell. All values in $A = 124$ – 130 are obtained from the current data set. The remaining values are taken from Refs. [2,3]. Note that in the configuration of the $19/2^+$ states above $N = 73$, $d_{3/2}$ and $s_{1/2}$ contributions are comparable. Lines in panel (b) are drawn to guide the eye.

- (i) The $19/2^+$ isomeric state has been reported in the mass chain $A = 119$ – 129 [10,11,44] with a dominant configuration of a $h_{11/2}^{-1}$ neutron hole orbital coupled to the 5^- core of the even Sn neighbor. Note that the 5^- state in the even Sn originates from a dominant $s_{1/2}^{-1}h_{11/2}^{-1}$ quasiparticle configuration, confirmed by g -factor measurements for the $^{116,118,120}\text{Sn}$ isomers [45]. The 5^- states are μ s isomers in ^{116}Sn [46] and ^{124}Sn [47] only, but these are ns isomers in the other even- A $^{118-122,128-130}\text{Sn}$ nuclei [48–52] because they can decay by $E1$ transitions to the 4^+ states lying just below them. However, in the odd- A isotopes, the $19/2^+$ states are all isomeric in the μ s range because each of them comes below the $(4^+ \otimes \nu h_{11/2})17/2^-$ and $19/2^-$ states. Therefore, the decay from these states must proceed by an $M2$ transition to the $(2^+ \otimes \nu h_{11/2})15/2^-$ state [11]. Note that $M2$ transitions in this model space can occur only between the orbitals $h_{11/2}$ and $g_{7/2}$, the latter of which lies deep below the Fermi level. According to SM calculations [42], the $\Delta I = 2$ parity changing transitions may have a comparable $E3$ width due to a $h_{11/2} \rightarrow d_{5/2}$ transition. In Ref. [10] large hindrance factors consistent with an $M2$ multipolarity are measured and a weak admixture of $h_{11/2}^{-2}g_{7/2}^{-1}$ was suggested, in agreement with SM calculations. Besides the aforementioned $s_{1/2}^{-1}h_{11/2}^{-1}$ component the SM yields a strong $d_{3/2}^{-1}h_{11/2}^{-1}$ amplitude in the $19/2^+$ that increases toward ^{129}Sn . The magnetic moment of this isomer in ^{127}Sn has been measured in this experimental campaign, and its result will shed more light on the configuration and the decay of the $19/2^+$ state in ^{127}Sn [53].
- (ii) The $23/2^+$ isomeric state has been previously observed in ^{123}Sn [2] and in the heavier $^{127-129}\text{Sn}$ [12,36] nuclei with a leading configuration of a neutron hole in

the $h_{11/2}$ orbital coupled to the 7^- core of the even Sn neighbor. All of the 7^- states are isomeric and have mostly $d_{3/2}^{-1}h_{11/2}^{-1}$ character. These states decay by $E2$ transitions to the 5^- states in the mass range $A = 118$ – 126 . In contrast, in ^{128}Sn and ^{130}Sn , where the 5^- is above the 7^- level, due to a reduced $s_{1/2}$ component in its wave function, the half-lives of the 7^- are well beyond the μ s range. The as-yet unobserved $23/2^+$ states in the lighter Sn isotopes are expected also to follow the trend of the 7^- states of their even partners and are a subject of future measurements.

- (iii) The $27/2^-$ isomeric state has been observed in the mass range $^{119-125}\text{Sn}$ [1,2,4] with a pure single-particle $h_{11/2}^{-n}$, seniority $\nu = 3$ configuration and predicted in the heavy $^{127-129}\text{Sn}$ with a sub- μ s half-life [10].

The experimental energy levels from the current work for a new ($23/2^+$) state in ^{125}Sn and new ($27/2^-$) states in $^{127,129}\text{Sn}$ are added to the systematics [Fig. 9(a)]. One sees a lowering of the excited states toward the doubly magic region. The energy spacing between the different states originates most probably from an admixture in the configurations, where one or another orbital contribution becomes dominant as, for example, at $A = 127$ – 128 .

E. SM and transition probabilities

The experimental reduced $E2$ transition probabilities for the 10^+ isomers in the even Sn isotopes extracted from the current data ($A \geq 124$) are compared to those of the $19/2^+$, $23/2^+$, and $27/2^-$ states in Fig. 9(b). The data points for $A < 124$ are taken from Refs. [2,3]. This plot shows the systematic trends of the $B(E2)$ values as the $h_{11/2}$ orbital is filled.

TABLE II. Reduced $I \rightarrow I - 2$ transition probabilities for the $19/2^+$, $23/2^+$, and $27/2^-$ isomers in ^{125}Sn , ^{127}Sn , and ^{129}Sn . The conversion coefficients used are taken from Ref. [55].

Nucleus	I^π	$B(E2)(e^2 \text{ fm}^4)$			
		Literature	This work	Adopted	SM
^{125}Sn	$27/2^-$	18(2) ^a	17.5(16)	17.7(12)	6.1
^{125}Sn	$23/2^+$	—	5.7(21)	5.7(21)	8.5
^{125}Sn	$19/2^+$	18(3) ^b	20.5(6)	20.4(6)	11.6
^{127}Sn	$27/2^-$	—	26.8(32)	26.8(32)	28.2
^{127}Sn	$23/2^+$	15.2(20) ^c	20.8(59)	15.8(19)	21.8
^{127}Sn	$19/2^+$	34(4) ^b , 34(3) ^c	40.8(12)	39.4(11)	30.1
^{129}Sn	$27/2^-$	—	30.7(122)	30.7(122)	21.9
^{129}Sn	$23/2^+$	50(6) ^c , 48(4) ^d	50.1(85)	48.8(31)	38.4
^{129}Sn	$19/2^+$	32(2) ^b , 51(7) ^c , 53(3) ^d	58.8(71)	40.1(16)	64.4

^aFrom Ref. [1].

^bFrom Ref. [10].

^cFrom Ref. [36].

^dFrom Ref. [12].

The $B(E2)$ dependence on $\nu h_{11/2}$ subshell occupation in even- A and odd- A Sn nuclei was discussed in Refs. [1,2], where the experimental $E2$ matrix elements as inferred from the square root of $B(E2)$, adopting a sign convention that changes in mid-shell, have been plotted as a function of the mass number A . The updated version is shown in Fig. 10, where it can be seen that the new data points for $^{127,129}\text{Sn}$ match up smoothly with the results for the other isotopes. These results reinforce earlier conclusions about the $\nu h_{11/2}$ subshell filling and about the enhancement of the neutron effective charge toward the middle of the $N = 50$ – 82 major shell [2]. The smooth systematic trend exhibited by these seniority isomers reflects the quasispin tensorial structure of the $E2$

operator as established from abundant data in other subshells and regions of the Segré chart such as $N = 50(g_{9/2}^n)$, $82(h_{11/2}^n)$, and $126(h_{9/2}^n)$ isotones and Pb ($i_{13/2}^n$) isotopes. The presence of the $d_{3/2}$ shell leads to a delayed occupation of the $h_{11/2}$ shell close to ^{132}Sn .

The reduced $E2$ transition probabilities of the odd- A Sn isotopes, along with the corresponding transitions in the even- A nuclei, are compared to each other and SM results in Fig. 11 and Table II. One has to note that the half-lives and $B(E2)$ values of the present work for the even Sn isotopes agree well with the literature values [1,10,12,54]. In Fig. 11(a) the experimental and SM $B(E2)$ strengths for the $h_{11/2}^- \nu = 2$ configurations $10^+ \rightarrow 8^+$ (even A) and $\nu = 3$ $27/2^- \rightarrow 23/2^-$ (odd A) are compared. The odd- A values are scaled with a factor 0.264, which accounts for the different angular momentum recoupling factors for $\nu = 2$ and $\nu = 3$ configurations and normalizes the odd- A $B(E2)$ values to the average of the neighboring even- A strength [56]. In this way the trend with decreasing A reflects directly the emptying of the $h_{11/2}$ orbital [1,4]. The staggering at $A = 129$ is artificial as the normalization is inadequate beyond $A = 128$. This is due to the presence of the $d_{3/2}$ shell, which is emptied first before the $h_{11/2}$ orbital. From the $A = 128$ – 130 values one may conclude that the choice of an effective charge of $0.70e$, as taken from the literature [57], is probably on the low side and a value of $0.85e$ would be more appropriate [13,36]. This increase, however, would not cure the discrepancy observed toward mid-shell, which clearly indicates a too fast emptying of the $h_{11/2}$ orbital. For ^{125}Sn the leading components of the $27/2^-$ and $23/2^-$ wave functions are $d_{3/2}^{-2} h_{11/2}^{-3}$ and $h_{11/2}^{-3}$ with 45% and 12%, respectively. As the $E2$ matrix elements in the lowest seniority change sign in mid-shell, which reflects the shape change from prolate to oblate, the contributions of these two configurations interfere destructively. A reduction of the minority component to half its value would bring the theoretical value close to experiment. As pointed out in Sec. IV A, the weak $B(E2)$ values in the $h_{11/2}$ mid-shell are specifically sensitive to the neglect of proton-core excitations. This was demonstrated in the $N = 50$ isotones one major

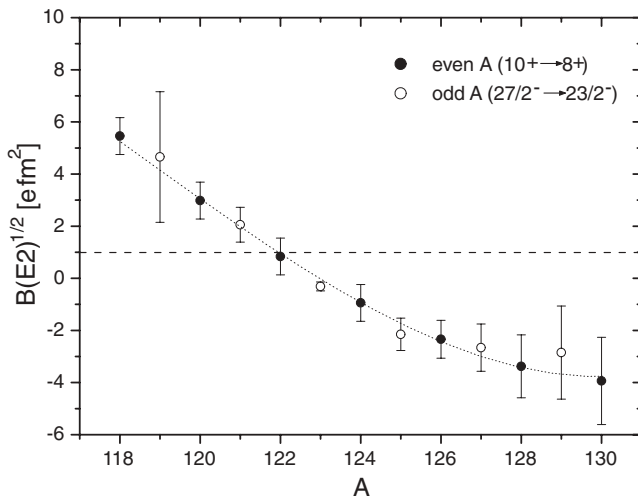


FIG. 10. Experimental $E2$ transition amplitudes for the $h_{11/2}^- \nu = 2$ ($10^+ \rightarrow 8^+$) and $27/2^-$ ($\nu = 3$) isomeric states in the Sn isotopes [with the odd- A values scaled by 0.514 to compensate for the different geometrical factors entering $\nu = 2$ and $\nu = 3$ $B(E2)$ equations]. All values in $A = 124$ – 130 are obtained from the current data set. The remaining values are taken from Refs. [2,3]. The dotted curve is drawn to guide the eye.

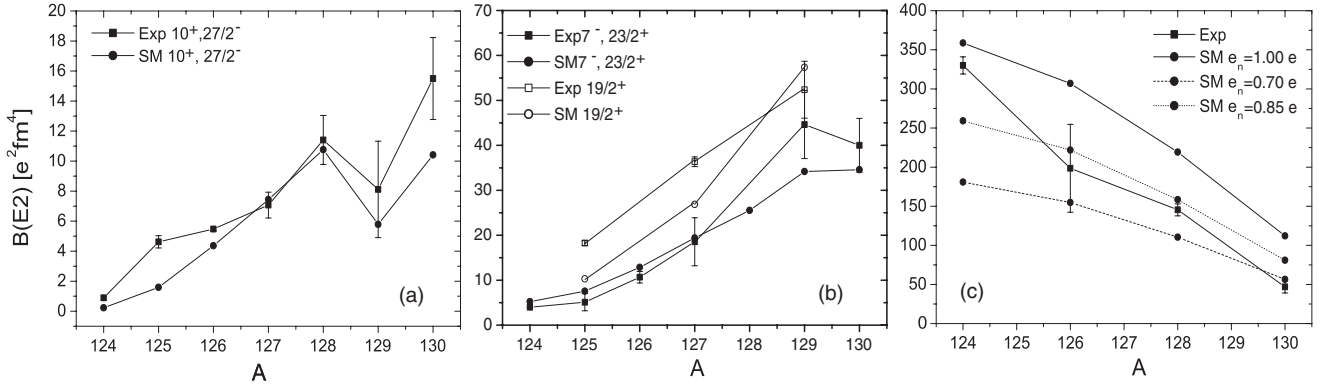


FIG. 11. Comparison between experimental and theoretical reduced transition probabilities for (a) the $h_{11/2}^{-n} 10^+(v=2)$ and $27/2^-(v=3)$ isomeric states in the heavy Sn isotopes [with the odd- A values scaled by 0.264 to compensate for the different geometrical factors entering $v=2$ and $v=3$ $B(E2)$ equations] and (b) mixed $h_{11/2}^{-n}(s, d)$ states. $B(E2; 5^- \rightarrow 7^-)$ in $^{128,130}\text{Sn}$ are converted into $B(E2; 7^- \rightarrow 5^-)$ for better comparison; the odd- A values are scaled by 0.891. The effective neutron charge is $0.70e$. SM (squares) and experimental $B(E2; 2^+ \rightarrow 0^+)$ (circles) [1,21,47,51,52] are shown in (c) for effective charges $e_n = 1.00e$ (solid line), $0.70e$ (dashed line), and $0.85e$ (dotted line).

shell below for $g_{9/2}$ protons [15,58]. Further SM tests of the $h_{11/2}^{-n}$ $B(E2)$ have revealed that the underestimation of the $^{125,126}\text{Sn}$ values can be cured by reducing the pairing two-body matrix elements (TBME) involving $h_{11/2}$, while the $B(E2)$ for the other configurations are virtually unchanged. The ^{124}Sn $10^+ \rightarrow 8^+$ transition is not affected, which supports the conclusion that deviations in the decreasing $B(E2)$ toward mid-shell for all transitions shown in Fig. 11 are due to the increasing influence of proton-core excitations.

In Fig. 11(b) the $E2$ transition strengths for the positive-parity yrast traps with mixed configuration $h_{11/2}^{-n}(s, d)$, $23/2^+$ and $19/2^+$, are compared to the $7^- \rightarrow 5^-$ strengths and SM results. Because of the changing configurational character of the states involved, a simple geometrical scaling of odd- A to even- A values is not meaningful. Therefore, the odd- A values are scaled to have equal values for the two- and three-hole isotopes, $^{130,129}\text{Sn}$. For ^{130}Sn the experimentally observed $5^- \rightarrow 7^-$ strength is converted to $7^- \rightarrow 5^-$. Again the values for $A = 129$ and 130 indicate a too small effective charge; the trend with decreasing mass number, however, is nicely reproduced by the SM. From the smooth trend of both experimental and SM values, the unobserved branch for the $5^- \rightarrow 7^-$ transition in ^{128}Sn can be estimated to be 0.2% [Fig. 11(b)]. The $19/2^+ \rightarrow 15/2^+$ $E2$ strengths below $A = 129$ seem to be systematically underestimated by the shell model. The situation for these nonstretched states resembles the 2^+ systematics [Fig. 11(c)], where the optimum effective charge changes from $0.70e$ to $1.00e$ from ^{130}Sn to ^{124}Sn in the present calculations. It seems that the value of $0.85e$ best describes the experimental values [21].

Proton-core excitation besides generally increasing effective charges will increase seniority mixing in configurations coupled to less than maximum spin due to the proton-neutron (pn) interaction. The $19/2^+$ and $15/2^+$ wave functions comprise of the $h_{11/2}^{\pm 4,6}$ configuration with two 6^+ and 8^+ states with $v = 2, 4$ within 150 keV, which will undergo increased mixing by virtue of pn interaction and, depending on the relative sign of the valence and core-excited contribution,

enable constructive or destructive interference of $\Delta v = 2$ contributions to the $E2$ matrix element. It should be noted that while the $\Delta v = 0$ strength disappears in mid-shell, the $\Delta v = 2$ transition strength peaks there (see, e.g., $2^+ \rightarrow 0^+$ transitions [15,21] (Fig. 2) for the $g_{9/2}^n$ system).

V. SUMMARY

In relativistic fission and fragmentation reactions several Sn isotopes in the vicinity of ^{132}Sn have been populated and their decay in the 0.2 to 14 μs range has been studied. The data allowed the observation of three new isomeric states in ^{125}Sn , ^{127}Sn , and ^{129}Sn . The new states have been suggested to have $I^\pi = (23/2^+)$ in ^{125}Sn and $(27/2^-)$ in ^{127}Sn and ^{129}Sn , based on theoretical calculations for the yrast traps in this high-spin region. The level schemes of these nuclei have been extended and, additionally, the transition probabilities for all isomeric states have been extracted.

Shell-model calculations in an untruncated $N = 50$ –82 neutron space give an excellent description of the experimental level schemes and their systematics with increasing distance from the doubly-magic ^{132}Sn . The evolution of the $E2$ strengths for transitions from the stretched and pure $h_{11/2}^{-n}$ $I^\pi = 27/2^-$, 10^+ seniority $v = 3, 2$ states toward mid-shell and from the mixed-orbital $I^\pi = 23/2^+, 7^-$, and $19/2^+$ isomers is well described. Deviations in the absolute values for small $B(E2)$ and transitions involving nonstretched configurations may be ascribed to the neglect of proton excitations across $Z = 50$, which can only be partly absorbed by the choice of a constant effective neutron charge of $e_n = 0.70e$. A variation from $0.70e$ at $N = 82$ to $1.00e$ at $N \sim 70$ might be more appropriate.

ACKNOWLEDGMENTS

The authors would like to thank M. Hjorth-Jensen for providing the original interaction two-body matrix elements. This work was supported in part by the EU, EURONS Contract

No. RII3-CT-2004-506065, the Flemish Science Foundation FWO Project No. G0446-05, the Belgian Science Policy IAP Project No. P6/23, the Bulgarian National Science Fund Grant No. VUF06/05, the Polish Ministry of Science and Higher Education Grant Nos. 1 P03B 03030 and 620/E-

77/SPB/GSI/P-03/DWM105/2004-2007, BMBF Contract No. 06KY205I, the Romanian National Authority for Scientific Research Contract No. 52/07, the Swedish Research Council, and the Spanish Ministerio de Educación y Ciencia Nos. FPA2005-00696 and FPA2007-66069.

-
- [1] C. T. Zhang, P. Bhattacharyya, P. J. Daly, Z. W. Grabowski, R. Broda, B. Fornal, and J. Blomqvist, *Phys. Rev. C* **62**, 057305 (2000).
- [2] R. Mayer, D. Nisius, I. Bearden, E. Bhattacharyya, L. Richter, M. Sferrazza, Z. Grabowski, E. Daly, R. Broda, B. Fornal *et al.*, *Phys. Lett.* **B336**, 308 (1994).
- [3] R. Broda, R. Mayer, I. Bearden, P. Benet, P. Daly, Z. Gabrowski, M. Carpenter, R. Janssens, T. Khoo, T. Lauritsen *et al.*, *Phys. Rev. Lett.* **68**, 1671 (1992).
- [4] P. J. Daly, R. Mayer, D. Nisius, I. Bearden, P. Bhattacharyya, L. Richter, M. Sferrazza, Z. Gabrowski, R. Broda, B. Fornal *et al.*, *Phys. Scr.* **T56**, 94 (1995).
- [5] M. Mineva, M. Hellström, M. Bernas, J. Gerl, H. Grawe, M. Pfützner, P. Regan, M. Rejmund, D. Rudolph, F. Becker *et al.*, *Eur. Phys. J. A* **11**, 9 (2001).
- [6] M. Hellström, M. Mineva, A. Blazhev, H. Boardman, J. Ekman, J. Gerl, K. Gladnishki, H. Grawe, R. Page, Z. Podolyak *et al.*, in *Proceedings of the International Workshop XXXI on Cross Properties of Nuclei and Nuclear Excitations, Hirschegg, Austria*, edited by H. Feldmeier, J. Knoll, W. Nörenberg, and J. Wambach (GSI Darmstadt, 2003), p. 72.
- [7] M. Hellström, M. Mineva, A. Blazhev, H. Boardman, J. Ekman, K. Gladnishki, H. Grawe, J. Gerl, R. Page, Z. Podolyak *et al.*, in *Proceedings of the Third International Conference on Fission and Properties of Neutron-Rich Nuclei*, Sanibel Island, Florida, USA, edited by J. Hamilton, A. Ramayya, and H. Carter (World Scientific, 2002), p. 22.
- [8] A. Jungclaus, L. Caceres, M. Gorska, M. Pfützner, S. Pietri, E. Werner-Malento, H. Grawe, K. Langanke, G. Martínez-Pinedo, F. Nowacki *et al.*, *Phys. Rev. Lett.* **99**, 132501 (2007).
- [9] N. Hoteling, W. Walters, B. Tomlin, P. Mantica, J. Pereira, A. Becerril, T. Fleckenstein, A. Hecht, G. Lorusso, M. Quinn *et al.*, *Phys. Rev. C* **76**, 044324 (2007).
- [10] J. A. Pinston, C. Foin, J. Genevey, R. Beraud, E. Chabanat, H. Faust, S. Oberstedt, and B. Weiss, *Phys. Rev. C* **61**, 024312 (2000).
- [11] J. A. Pinston and J. Genevey, *J. Phys. G: Nucl. Part. Phys.* **30**, R57 (2004).
- [12] J. Genevey, J. A. Pinston, C. Foin, M. Rejmund, H. Faust, and B. Weiss, *Phys. Rev. C* **65**, 034322 (2002).
- [13] B. Fogelberg, K. Heyde, and J. Sau, *Nucl. Phys.* **A352**, 157 (1981).
- [14] L. E. DeGeer and G. B. Holm, *Phys. Rev. C* **22**, 2163 (1980).
- [15] H. Grawe, *Lect. Notes Phys.* **651**, 33 (2004).
- [16] R. F. Casten, *Nuclear Structure from a Simple Perspective*, 2nd ed. (Oxford Univ. Press, New York, 2000), p. 153.
- [17] H. Geissel, P. Armbruster, K.-H. Behr, A. Brunle, K.-H. Burkard, M. Chen, H. Folger, B. Franczak, H. Keller, and O. Klepper, *Nucl. Instrum. Methods B* **70**, 286 (1992).
- [18] R. Machleidt, F. Sammarruca, and Y. Song, *Phys. Rev. C* **53**, R1483 (1996).
- [19] L. Coraggio, A. Covello, A. Gargano, and N. Itaco, *Phys. Rev. C* **65**, 051306(R) (2002).
- [20] J. Shergur, B. Brown, V. Fedoseyev, U. Koester, K.-L. Kratz, D. Seweryniak, W. Walters, A. Woehr, D. Fedorov, M. Hannawald *et al.*, *Phys. Rev. C* **65**, 034313 (2002).
- [21] A. Banu, J. Gerl, C. Fahlander, M. Gorska, H. Grawe, T. Saito, H.-J. Wollersheim, E. Caurier, T. Engeland, A. Gniady *et al.*, *Phys. Rev. C* **72**, 061305(R) (2005).
- [22] J. Eberth, H. Thomas, P. von Brentano, R. Lieder, H. Jäger, H. Kämmerling, M. Berst, D. Gutknecht, and R. Henck, *Nucl. Instrum. Methods A* **369**, 135 (1996).
- [23] H.-J. Wollersheim, D. Appelbe, A. Banu, R. Bassini, T. Beck, F. Becker, P. Bednarczyk, K.-H. Behr, M. Bentley, G. Benzoni *et al.*, *Nucl. Instrum. Methods A* **537**, 637 (2005).
- [24] G. Neyens, L. Atanasova, D. Balabanski, F. Becker, P. Bednarczyk, L. Caceres, P. Doornenbal, J. Gerl, M. Gorska, J. Grebosz *et al.*, *Acta Phys. Pol. B* **38**, 1237 (2007).
- [25] L. Atanasova, D. Balabanski, M. Hass, F. Becker, P. Bednarczyk, S. Chamoli, P. Doornenbal, G. Georgiev, J. Gerl, K. Gladnishki *et al.*, *Prog. Part. Nucl. Phys.* **59**, 355 (2007).
- [26] M. Wilhelm, J. Eberth, G. Pascovici, E. Radermacher, P. von Brentano, H. Prade, and R. Lieder, *Nucl. Instrum. Methods A* **381**, 462 (1996).
- [27] B. Herskind, *J. Phys. (Paris) Colloq.* **41**, C10, 106 (1980).
- [28] D. Radford, *Nucl. Instrum. Methods A* **361**, 306 (1995).
- [29] M. Bhat, *Nucl. Data Sheets* **68**, 579 (1993).
- [30] R. Bunting and J. Kraushaar, *Nucl. Instrum. Methods* **118**, 565 (1974).
- [31] K. Kossert and E. Guenther, *Appl. Radiat. Isot.* **60**, 459 (2004).
- [32] J. Grebosz, *Comput. Phys. Commun.* **176**, 251 (2007).
- [33] ROOT, www.root.cern.ch
- [34] RADWARE, radware.phy.ornl.gov
- [35] W.-T. Chou and M. King, *Nucl. Data Sheets* **73**, 215 (1994).
- [36] H. Gausemel, B. Fogelberg, T. Engeland, M. Hjorth-Jensen, P. Hoff, H. Mach, K. A. Mezilev, and J. P. Omtvedt, *Phys. Rev. C* **69**, 054307 (2004).
- [37] B. Fogelberg and P. Carle, *Nucl. Phys.* **A323**, 205 (1979).
- [38] M. Hjorth-Jensen, T. Kuo, and E. Osnes, *Phys. Rep.* **261**, 125 (1995).
- [39] H. Grawe, K. Langanke, and G. Martínez-Pinedo, *Rep. Prog. Phys.* **70**, 1525 (2007).
- [40] O. Kavatsyuk, C. Mazzocchi, Z. Janas, A. Banu, L. Batist, F. Becker, A. Blazhev, W. Brüche, J. Döring, T. Faestermann *et al.*, *Eur. Phys. J. A* **31**, 319 (2007).
- [41] B. Brown, A. Etchegoyen, W. R. N. Godwin, W. Richter, W. Orman, E. Warburton, J. Winfield, L. Zhao, and C. Zimmerman, OXBASH for Windows, MSU-NSCL Report No. 1289, 2004.
- [42] H. Grawe *et al.* (to be published).
- [43] S. Pietri *et al.* (in preparation).
- [44] R. Mayer, B. Fornal, R. Broda, I. Beardcn, Z. Grabowski, S. Lunardi, T. Lauritsen, M. Carpenter, R. Janssens, T. L. Khoo *et al.*, *Z. Phys. A* **342**, 247 (1992).
- [45] N. Stone, *At. Data Nucl. Data Tables* **90**, 75 (2005).

- [46] J. Blachot, Nucl. Data Sheets **92**, 455 (2001).
- [47] H. Iimura, J. Katakura, K. Kitao, and T. Tamura, Nucl. Data Sheets **80**, 895 (1997).
- [48] K. Kitao, Nucl. Data Sheets **75**, 99 (1995).
- [49] K. Kitao, Y. Tendow, and A. Hashizume, Nucl. Data Sheets **96**, 241 (2002).
- [50] T. Tamura, Nucl. Data Sheets **108**, 455 (2007).
- [51] M. Kanbe and K. Kitao, Nucl. Data Sheets **94**, 227 (2001).
- [52] B. Singh, Nucl. Data Sheets **93**, 33 (2001).
- [53] L. Atanasova *et al.* (in preparation).
- [54] B. Fogelberg, H. Gausemel, K. Mezilev, P. Hoff, H. Mach, M. Sanchez-Vega, A. Lindroth, E. Ramström, J. Genevey, J. Pinston *et al.*, Phys. Rev. C **70**, 034312 (2004).
- [55] T. Kibedi, T. W. Burrows, M. B. Trzhaskovskaya, P. M. Davidson, and C. W. Nestor, Nucl. Instrum. Methods A **589**, 202 (2008).
- [56] J. H. McNeill, J. Blomqvist, A. A. Chishti, P. J. Daly, W. Gelletly, M. A. C. Hotchkis, M. Piiparinen, B. J. Varley, and P. J. Woods, Phys. Rev. Lett. **63**, 860 (1989).
- [57] A. Holt, T. Engeland, M. Hjorth-Jensen, and E. Osnes, Nucl. Phys. **A634**, 41 (1998).
- [58] H. Grawe, A. Blazhev, M. Gorska, R. Grzywacz, H. Mach, and I. Mukha, Eur. Phys. J. A **27**, s01, 257 (2006).